Vertical escape tactics and movement potential of orthocone cephalopods

David Peterman [Corresp., 1], **Kathleen Ritterbush** [1]

[1] Department of Geology and Geophysics, University of Utah, Salt Lake City, Utah, United States

Corresponding Author: David Peterman
Email address: David.Peterman@utah.edu

Measuring locomotion tactics available to ancient sea animals can link functional morphology with evolution and ecology over geologic timescales. Externally-shelled cephalopods are particularly important for their central roles in marine trophic exchanges, but most fossil taxa lack sufficient modern analogues for comparison. In particular, phylogenetically diverse cephalopods produced orthocone conchs (straight shells) repeatedly through time. Persistent re-evolution of this morphotype suggests that it possesses adaptive value. Practical lateral propulsion is ruled out as an adaptive driver among orthocone cephalopods due to the stable, vertical orientations of taxa lacking sufficient counterweights. However, this constraint grants the possibility of rapid (or efficient) vertical propulsion. We experiment with this form of movement using 3D-printed models of *Baculites compressus*, weighted to mimic hydrostatic properties inferred by virtual models. Furthermore, model buoyancy was manipulated to impart simulated thrust during four scenarios (*Nautilus*-like cruising thrust; a similar thrust scaled by the mantle cavity of *Sepia*; sustained peak *Nautilus*-like thrust; and passive, slightly negative buoyancy). Each model was monitored underwater with two submerged cameras as they rose/fell over ~2 meters, and their kinematics were computed with 3D motion tracking. Our results demonstrate that orthocones require very low input thrust for high output in movement and velocity. With *Nautilus*-like peak thrust, the model reaches velocities of 1.2 m/s (2.1 body lengths per second) within one second starting from a static initial condition. While cephalopods with orthocone conchs likely assumed a variety of life habits, these experiments illuminate some first-order constraints. Low hydrodynamic drag inferred by vertical displacement suggests that vertical migration would incur very low metabolic cost. While these cephalopods likely assumed low energy lifestyles day-to-day, they may have had a fighting chance to escape from larger, faster predators by performing quick, upward dodges. The current experiments suggest that orthocones sacrifice horizontal mobility for highly streamlined, vertically-stable, upwardly-motile conchs. Repeated evolution of this unique form could signal times of ecological saturation of other biomechanical modes

among concomitant cephalopod faunas, and/or ecological opportunity (to escape relevant predators).

Vertical escape tactics and movement potential of orthocone cephalopods

David Joseph Peterman[1], Kathleen Anita Ritterbush[1]

[1] Department of Geology and Geophysics, University of Utah, Salt Lake City, Utah, USA

Corresponding Author:
David J. Peterman[1]
115, Salt Lake City, UT 84112, USA
Email address: David.Peterman@utah.edu

Abstract

Measuring locomotion tactics available to ancient sea animals can link functional morphology with evolution and ecology over geologic timescales. Externally-shelled cephalopods are particularly important for their central roles in marine trophic exchanges, but most fossil taxa lack sufficient modern analogues for comparison. In particular, phylogenetically diverse cephalopods produced orthocone conchs (straight shells) repeatedly through time. Persistent re-evolution of this morphotype suggests that it possesses adaptive value. Practical lateral propulsion is ruled out as an adaptive driver among orthocone cephalopods due to the stable, vertical orientations of taxa lacking sufficient counterweights. However, this constraint grants the possibility of rapid (or efficient) vertical propulsion. We experiment with this form of movement using 3D-printed models of *Baculites compressus*, weighted to mimic hydrostatic properties inferred by virtual models. Furthermore, model buoyancy was manipulated to impart simulated thrust during four scenarios (*Nautilus*-like cruising thrust; a similar thrust scaled by the mantle cavity of *Sepia*; sustained peak *Nautilus*-like thrust; and passive, slightly negative buoyancy). Each model was monitored underwater with two submerged cameras as they rose/fell over ~2 meters, and their kinematics were computed with 3D motion tracking. Our results demonstrate that orthocones require very low input thrust for high output in movement and velocity. With *Nautilus*-like peak thrust, the model reaches velocities of 1.2 m/s (2.1 body lengths per second) within one second starting from a static initial condition. While cephalopods with orthocone conchs likely assumed a variety of life habits, these experiments illuminate some first-order constraints. Low hydrodynamic drag inferred by vertical displacement suggests that vertical migration would incur very low metabolic cost. While these cephalopods likely assumed low energy lifestyles day-to-day, they may have had a fighting chance to escape from larger, faster predators by performing quick, upward dodges. The current experiments suggest that orthocones sacrifice horizontal mobility for highly streamlined, vertically-stable, upwardly-motile conchs. Repeated evolution of this unique form could signal times of ecological saturation

of other biomechanical modes among concomitant cephalopod faunas, and/or ecological opportunity (to escape relevant predators).

Introduction

A phylogenetically-diverse array of cephalopod mollusks produced straight conchs (orthocones) throughout geologic time, but their ecological contributions to marine systems are unclear. The evolutionary contexts of these animals are well documented: iconic spiral conchs of nautilids (extant) and ammonoids (extinct) are heavily-derived forms that follow early success by orthocone relatives. Orthocone nautiloids were globally distributed and diverse in the Paleozoic, yielding hundreds of fossil genera (*Teichert et al., 1964*). A branch of orthocerid nautiloids gave rise to orthoconic bactritoids, and eventually to ammonoids (*Erben, 1966; Monnet, Klug, and De Baets, 2015*). Evolution of tightly-coiled ammonoid conchs in Early Devonian seas (by increased exogastric curvature; *Klug and Korn, 2004; Kröger and Mapes, 2007; Monnet, De Baets, and Klug, 2011*) may have radically increased horizontal mobility via hydrostatic and hydrodynamic features (aligning jet thrust to the animal's center of mass while simultaneously improving lateral streamlining; *Klug and Korn, 2004*). Yet orthocone nautiloid lineages persisted until the Late Triassic, and orthocone ammonoids repeatedly originated from planispiral ancestors through the Mesozoic (e.g., heteromorph species within Triassic Choristoceratidae, Jurassic Spiroceratidae, Late Jurassic/Early Cretaceous Bochianitidae, and Cretaceous Baculitidae; *Wiedmann, 1969; Wright, Callomon, and Howarth, 1996; Hoffmann et al., 2021*). Intermittent appearance of orthocone forms suggests that this morphotype retained adaptive value, despite proliferation of planispiral conchs among these animals' contemporaries. However, the adaptive value, functional morphology, and ecology of orthocone cephalopods are poorly understood. We aim to investigate these properties through hydrostatic and hydrodynamic analyses using the Cretaceous baculitid, *Baculites compressus* (North America, Late Campanian), as a test case.

Hydrostatics of orthocone cephalopods

Hydrostatic analyses suggest that orthocone cephalopods assumed vertical orientations at rest (*Trueman, 1941; Westermann, 1977, 1996; Peterman et al., 2019; Peterman, Barton, and Yacobucci, 2019*). Mass would be anteriorly distributed near the body chamber (housing the animal's soft body) due to the overlying air-filled chambers (the phragmocone buoyancy apparatus). A static orientation occurs when the total center of mass is vertically aligned under the center of buoyancy (*Hoffmann et al., 2015*). When these centers are forced out of alignment, a restoring moment proportionate to their separation will act to return them to their static, equilibrium condition (*Peterman et al., 2019; Peterman et al., 2020a; Peterman et al., 2020b*). Mineral deposits (i.e., cameral and endosiphuncular deposits) common among some Paleozoic nautiloid species may form counterweights that altered restoring moments and dynamic conch orientation, though static orientation would likely remain near vertical (*Peterman, Barton, and Yacobucci 2019)*.

Hydrostatic and hydrodynamic relationships (*Peterman et al., 2019; Peterman, Barton, and Yacobucci, 2019*) contrast interpretations of orthocone cephalopods as swift horizontal swimmers, akin to extant squid (*Tsujita and Westermann, 1988*). First, the source of jet thrust (i.e., the hyponome) is aligned vertically with the centers of buoyancy and mass (*Peterman et al., 2019*), supporting that thrust energy would most efficiently be transmitted into upward vertical movement during jet propulsion. If thrust was applied in a horizontal direction, much energy would be lost to rocking since the source of jet thrust is situated much lower than these two hydrostatic centers (*Peterman et al., 2019)*. Moreover, thrust perpendicular to the long axis of the conch would not be sufficient to orient the animal horizontally (*Peterman et al., 2019*). These properties strongly constrained how orthocone cephalopods would have interacted with their surroundings, fed, and evaded predators. The source of thrust relative to the mass distribution and vertically streamlined conch suggest that orthocones were adapted for improved vertical movement potential, but at the expense of horizontal mobility.

Orthocone cephalopod paleoecology

Constraining likely locomotory functions for orthocone cephalopods can lend context to a very diverse range of lineages that flourished throughout the Paleozoic and Mesozoic, and are known from nearly all marine paleoenvironments around the globe (*Kennedy and Cobban, 1976; Wright, Callomon, and Howarth, 1996; Kröger and Zhang, 2009; Kröger, Servais, and Zhang, 2009*). Orthocone nautiloids are generally regarded as vertical migrants of the water column based on occurrence data, morphological characters, and taphonomic patterns (*Kröger, Servais, and Zhang, 2009*). Species recovered from offshore sediments may have migrated vertically through pelagic landscapes of varied photic and oxygen zones; whereas species recovered from more coastal deposits may have remained in the neritic zone where demersal feeding would be available (*Kröger, Servais, and Zhang, 2009*).

Orthocone ammonoids, in contrast, are generally found in neritic and epicontinental settings (*Kennedy and Cobban, 1976; Wright, Callomon, and Howarth, 1996*). The depth range of baculitid ammonoids was around 50-100 m based on isotopic analyses of well-preserved shell material (*Fatherree, Harries, and Quinn, 1998; Lukeneder et al., 2010; Henderson and Price, 2012; Lukeneder, 2015; Sessa et al., 2015; Landman et al., 2018; Hoffmann et al., 2021*). A demersal life habit is generally inferred from these analyses due to their isotopic similarity with the benthos (*Landman et al., 2018; Ferguson et al., 2019; Hoffmann et al., 2021*). Isotopic studies also suggest that some baculitids spent most of their lives at methane seeps, supporting a somewhat sedentary lifestyle (*Landman et al., 2018; Rowe et al., 2020*). However, baculitid associations with streamlined midwater swimmers and occurrences in deposits lacking demersal taxa suggest that these species could cope with life higher in the water column as well (*Tsujita and Westermann, 1998; Landman, Cobban, and Larson, 2012*).

Key observations remain that suggest horizontal (or subvertical) modes were adopted by at least some species of orthocone cephalopods. Life habit can be inferred from color patterns preserved on the conch. While some orthocones had color patterns around the entire

circumference, others have patterns restricted to the dorsum, suggesting countershading in a nonvertical orientation (*Packard, 1988; Westermann, 1998; Kröger, Servais, and Zhang, 2009; Manda and Turek, 2015*). These orientations can be explained by resting the soft body on the benthos (*Flower, 1955*) or by the use of active locomotion. The former would require some amount of negative buoyancy and would only provide useful camouflage from above, while the latter would require sustained jet thrust of considerable magnitude in forms with lower hydrostatic stability (i.e., those with cameral or endosiphuncular deposits; *Peterman, Barton, and Yacobucci, 2019*). Contrasting hydrostatic interpretations, aperture-forward, horizontal movement was inferred for the baculitid ammonoid, *Sciponoceras*, based on the adoral growth direction of a cirripede attached to the venter (*Hauschke, Schöllmann, and Keupp, 2011*).

While a single mode of life should not be invoked for all orthocone cephalopods, their life habit and ecology can be further constrained through empirical studies. The model ammonoid, *Baculites compressus*, can provide valuable insight for the vertical movement potential and kinematics of this hydrostatically stable morphotype. While the anatomy and propulsive capabilities likely varied within and between ammonoid and nautiloid groups, a wide range of experimental conditions allow broader interpretations for this morphotype as a whole. The ease or difficulty in vertical movement, similar to the behavior observed in extant nautilids (*Ward et al., 1984; Ward, 1987; O'Dor et al., 1993; Dunstan, Ward, and Marshall, 2011*) is of interest. Furthermore, the conditions required to vertically dodge larger, faster, predators with more speed-efficient modes of locomotion (undulatory vs jet propulsion; *Wells and O'Dor, 1986; Anderson and Grosenbaugh, 2005; Neil and Askew, 2018*) are explored with a range of predator analogues. An investigation of these capabilities can yield clues regarding the adaptive value of this enigmatic morphotype and its iterative recurrence in the fossil record.

Materials & Methods

Three-dimensional motion tracking was performed on physical models of *Baculites compressus* in order to investigate various hydrodynamic properties of the orthocone morphotype. These models were constructed from the virtual hydrostatic model of *Peterman et al. (2019)* (Fig. 1A). The exterior portion of this model was isolated in Blender (*Blender Online Community, 2017*), then a soft body more closely resembling the baculitid reconstruction of *Klug, Riegraf, and Lehmann (2012)* was fabricated and affixed to the aperture using the same software (Fig. 1B). The coiled embryonic shell (ammonitella) was ignored due to its very small scale (~0.7 mm; *Landman, 1982*). Instead, the model tapers to a point approximately 0.7 mm in diameter. The *Baculites compressus* model in the current study was designed to have positive or negative buoyant forces that simulate movement in the vertical directions using similar methods to *Peterman et al. (2021a)*. Each model in the current study was constructed at a size of 57 cm (from the conch apex to distal ends of the arms). An external 3D model of *Baculites compressus* is stored in the morphosource.org database (ark:/87602/m4/359359).

Vertical movement scenarios

Differences between the mass of water displaced and total model mass were computed to equal the forces produced during movement under four different scenarios: (1) *Nautilus*-like cruising thrust, (2) *Nautilus*-like cruising thrust scaled by the mantle cavity ratio of extant cuttlefish, (3) sustained maximum *Nautilus*-like thrust, and (4) slightly negative buoyancy similar to extant *Nautilus*. For Scenario 1, the thrust of 0.015 N required for a 73 g *Nautilus* to overcome drag at its maximum velocity (*Chamberlain, 1987*) was scaled by the mass of the water displaced by the current orthocone model (212.209 g) to yield a target thrust value of 0.0436 N. The mass of water displaced is equal to organismal mass, assuming a neutrally buoyant condition. This *Nautilus*-like thrust was then scaled from the mantle cavity ratio of *Nautilus* (0.15; *Wells and O'Dor, 1991*) to the mantle cavity ratio of *Sepia* (0.25; *Wells and O'Dor, 1991*) yielding a target thrust of 0.0727 N for Scenario 2. The maximum propulsive thrust for *Nautilus* is a function of body size (*Chamberlain, 1987*). For Scenario 3, this maximum thrust was computed by substituting the mass of the *Baculites compressus* model (212.209 g) into the following formula reported by *Chamberlain (1987)*:

$$T_{max} = 0.0021(m) - 0.103 \quad (1)$$

Where T_{max} is the maximum propulsive thrust in Newtons and m is the organismal mass in grams.

The model for Scenario 4 was made slightly negatively buoyant with a similar magnitude observed in extant *Nautilus*. *Ward and Martin (1978)* report residual masses (not relieved by buoyancy) for several wild caught *Nautilus*. Focusing on larger individuals from their study (>300 g), the average residual mass was 1.76 g with an average total mass of 676.6 g (~0.26% of their organismal mass is not relieved by buoyancy). This corresponds to a residual mass of 0.552 g for the orthocone model. In order to manage error, the model mass for this scenario was lowered by 1 g. The model was then made neutrally buoyant by adding liquid into an anterior chamber with a syringe through a self-healing rubber cap. Once the model no longer sank or rose for ~30 seconds, it was considered neutrally buoyant. Then the residual mass of 0.5 g was added with water through the syringe to make the model negatively buoyant according to the computed value.

Each target buoyant force depends on the mass of the water displaced by the models, which depends on density. Water density (1.000 g/cm^3) was computed with a calibrated 100 ml pycnometer using water from where the motion tracking experiments were conducted (described below).

Baculites compressus model construction

Each model is composed of three parts (Fig. 1B); air-filled voids, PLA (polylactic acid) plastic, and bismuth counterweights. Since the virtual models of these components are only digital volumes, their densities were determined with a calibrated 100 ml pycnometer to compute their masses. Virtual models of the counterweights were placed anteriorly (within the arm crown) with fixed positions and volumes for each model. After determining an appropriate counterweight volume (and therefore mass) for each model, the volumes of the internal voids

were adjusted to yield the proper total mass for each model. The positions of the voids were iteratively altered to maintain the same total model mass, while imparting the same hydrostatic stability index (0.505) and apex-upward orientation inferred from the virtual hydrostatic model (*Peterman et al., 2019*). The virtual models were considered finished when their hydrostatic stabilities and thrusts matched their target values to the third and fourth decimal places, respectively.

Hydrostatic stability indices were computed from the total center of mass and the center of buoyancy. The center of buoyancy was computed from the model of the exterior interface (i.e., a model of the water displaced). This center and the centers of mass for each material of unique density (air, water, PLA plastic, bismuth counterweight), were computed in MeshLab (*Cignoni and Ranzuglia, 2014*). The total center of mass was computed with the following formula:

$$M = \frac{\Sigma(D * m_o)}{\Sigma m_o} \quad (2)$$

Where M is the total center of mass in a principal direction, D is the center of mass of a single object in each principal direction, and m_o is the mass of any object of unique density. All coordinates are measured relative to the same arbitrary datum placed at the center of the aperture.

The hydrostatic stability index (S_t) was computed from the following equation:

$$S_t = \frac{D_{BM}}{\sqrt[3]{V}} \quad (3)$$

Where D_{BM} is the distance between the center of buoyancy (B) and the center of mass (M), computed with the 3D theorem of Pythagoras. V is the organismal volume (equal to the volume of water displaced).

The mass distribution of the PLA plastic required to impart the desired hydrostatic stability index was computed with the following formula:

$$D_{PLA} = \frac{M(m_{PLA} + m_{Bi} + m_{air} + m_{water}) - (D_{Bi}m_{Bi}) - (D_{air}m_{air}) - (D_{water}m_{water})}{(m_{PLA})} \quad (4)$$

Where D_{PLA} is the location of the PLA center of mass from the datum in each principle direction. M is the total center of mass in a particular principle direction, m is the mass of a model component, and D is the center of mass of each model component in a particular principle direction. Subscripts denote each model component. Water is present only in the negatively buoyant model (1 g).

After each virtual model was completed, they were 3D printed in a vertical orientation with an Ultimaker S5 in four parts (in order to fit within the available print volume). Each part contained a watertight void (Fig. 1B) that was sealed during 3D printing. Each of the four parts were chemically welded together with dichloromethane. High heat silicone molds of the counterweights were cast from 3D prints. The counterweights were cast form these molds by heating bismuth in a casting ladle with a propane torch, and evenly pouring the molten bismuth into the mold. The counterweights were further processed by using a metal file and silicon carbide paper until the desired volume and mass was reached. The counterweight masses slightly differed from their virtual counterparts because they were used to compensate for subtle

differences between the virtual and actual masses of the 3D printed parts. This modification minimized error of the target masses at the expense of error in hydrostatic stabilities. The hydrostatic stability indices of the physical models were recomputed with Equation 3, and all model components (aside from air) were weighed in grams to the third decimal place in order to report error in stability and simulated thrust. Tracking points were painted on the apex and the distal end of the arms for each final model (Fig. 1C) to monitor their position with motion tracking.

Motion tracking experiments

An underwater camera rig was designed to record video footage of the orthocone models as they rose/fell in the water (Fig. 2A). Experiments were performed in a seven-foot-deep section of the crimson lagoon – a 50 meter lap pool at the University of Utah. The skeleton of the rig was constructed with two-inch PVC pipe with custom 3D-printed fittings for two camera mounts. Three steel counterweights were position at each end of the T-shaped rig and rubber mats were wrapped around each section to prevent the rig from slipping on the pool liner. Each camera mount consists of a GoPro Hero 8 Black camera in a waterproof case on top of a waterproof LED light (Fig. 2B). Each camera was oriented with the long axis in the vertical direction for improved field of view. Videos were recorded at 60 frames per second with a linear field of view and 4K resolution. Each model was held with extendable tongs until steady, then released for a total of 15 trials for the positively buoyant scenarios, and 8 trials for the negatively buoyant scenario. The relationship between model texture and velocity were assessed by coating the orthocone model with peak *Nautilus*-like thrust (Scenario 3) with hydrophobic silicone spray and performing an additional 15 trials.

Dual video footage was imported into the 3D motion tracking software DLTdv8 (*Hedrick, 2008*) and semi-automatic tracking was used to mark the pixel locations of each tracking point (apex and arms). A calibration was performed in easyWand5 (*Theriault et al., 2014*) to transform the 2D pixel coordinates from each video into a single set of 3D coordinates in meters. The model itself was used for wand calibration, ensuring any 3D orientation of the model yielded its actual body length (57 cm). Three-dimensional data points higher in the water column were subject to minor image artifacts from light interacting with the water surface. These distortions in addition to the increasingly oblique apparent angles of each model yielded higher error in these regions. Calibrations with standard deviations of less than 2 cm were considered acceptable. The very fast frame rate (60 fps) caused fluctuations in velocity at lower time steps. This was remediated by using a moving average with a window of 11 time steps for the positively buoyant experiments. No moving average was used on the negatively buoyant experiment because only every 10th frame was used to compute velocity (due to very low velocities and long trial times).

Velocities were computed as a function of time for each model using the calibrated, 3D datapoints:

$$V_i = \frac{\sqrt{(x_i - x_{i-1})^2 + (y_i - y_{i-1})^2 + (z_i - z_{i-1})^2}}{(t_i - t_{i-1})} \quad (5)$$

Where V and t are velocity and time, and the subscripts i and i-1 refer to the current and previous time steps, respectively. The 3D theorem of Pythagoras was used to compute the total distance traveled in any x,y,z direction between time steps (which was mostly vertical). The video frame number was divided by the frame rate (59.94 frames per second) to compute time. Time zero for each trial was defined as the moment the release mechanism no longer contacted the model.

The curve fitting toolbox in MATLAB R2020a was used fit the velocity data for each model with an asymptotic equation in the form:

$$V_{fit} = a - ae^{-bt} \quad (6)$$

Where V_{fit} is the fit velocity and t is time. The term "a" is a coefficient denoting the velocity asymptote (i.e., the maximum velocity estimate given a particular thrust), and b is a coefficient that governs slope.

The relationships between hydrostatic stability and hydrodynamic movement were assessed by computing the maximum angle displaced from the vertical static orientation in any particular direction (θ_{dv}):

$$\theta_{dv} = \cos^{-1}\left(\frac{(z_2 - z_1)}{\sqrt{(x_2 - x_1)^2 + (y_2 - y_1)^2 + (z_2 - z_1)^2}}\right) \quad (7)$$

Where the subscripts 2 and 1 of the x, y, and z coordinates refer to the apical and arm tracking points, respectively.

Predator evasion potential

By knowing how velocity increases from stationary initial conditions (Equation 6), the time it takes to move one body length (t_{bl}) or half a body length ($t_{bl/2}$) can be computed:

$$\Delta P = L_{body} = \int_0^{t_{bl}} a - ae^{-bt} \quad (8)$$

When the change in position (ΔP) is equal to the length of the body (L_{body}; 57 cm), t_{bl} can be computed by integrating Equation 6 and determining the upper limit of integration. This limit was computed iteratively in MATLAB by increasing t_{bl} until the integrated equation was equal to L_{body}. For an orthocone to dodge a horizontally moving predator, jetting at the last moment would be ideal for a vertical escape. The minimum distance required (D) to dodge a predator attack at some incident velocity (V_p) was computed by multiplying t_{bl} or $t_{bl/2}$ by the predator's velocity (V_p). Since the critical swimming speeds of extinct animals are difficult to determine, extant marine predators were used as analogues.

Results

Model hydrostatics and error

Each of the four orthocone models have the same centers of buoyancy because their external volumes are identical (Table 1). However, the centers of mass for each component of unique density differed in order to maintain a stability index of 0.505 as total mass varied between models (Tables 1 and 2). The mass of the bismuth counterweights slightly differed from

their virtual counterparts to compensate for differences in mass between the virtual and physical PLA components. This mass difference reduced error in total mass by sacrificing accuracy in hydrostatic stability (Table 3). The differences in PLA mass were likely a result of differences in bulk density between each of the models. Even with identical slicer settings, the path of the extruder in each layer was slightly different between models, which contributed to error in PLA mass and density. Percent difference of hydrostatic stability and thrust between the virtual and physical models is reported on Table 3.

Motion tracking kinematics

The upward force on the physical models occurs on the center of buoyancy, not the location of the hyponome. However, this is a reasonable assumption for these experiments because perfect upward-vertical thrust is still simulated. Furthermore, the actual source of thrust and the centers of buoyancy and mass are very close to being vertically aligned in living orthocone cephalopods and in the current models. This alignment would allow thrust to be transmitted into primarily upward translation with little energy lost to rocking.

After releasing the models underwater, they primarily moved in the vertical directions with velocities proportionate to their simulated thrust values. Each of the trials were slightly skewed in the horizontal directions due to weak currents created by removing the release mechanism (Fig. 3). Additionally, the initial angles of some trials were slightly tilted from vertical, causing a few outlier trajectories (see Fig. 3A).

During vertical movement, high hydrostatic stability prevented substantial displacements from vertical orientations (Fig. 4). The tracking points were about two degrees from true vertical in a static setting, and most trials remained under five degrees from vertical. Larger angles of displacement were usually the result of a tilted starting position (see Fig. 4A). The negatively buoyant model underwent larger displacements from vertical only at higher velocities (~-7 cm/s) and consistently tilted dorsum-upwards.

The velocities between all trials of each positively buoyant model were remarkably similar (Fig. 5A-C). However, the negatively buoyant model (Fig. 5D) was more sensitive to initial conditions (i.e., the subtle motion caused by holding the tongs before and during release) due to the relatively low force acting in the downwards direction. While Equation 6 yields high R-squared values (>0.97), it underpredicts velocities at the start and end of the experiments, and slightly overpredicts velocities in the middle. This equation, however, provides a simple model to estimate orthocone swimming velocities using only a few terms (Table 4) and avoids overfitting the data. The velocity asymptote for each positively buoyant model is reported in Table 4. With sustained peak *Nautilus*-like thrust, the orthocone model reaches 1.2 m/s (2.1 body length per second) within one second from a stationary initial condition (Fig. 5C; Table 4). A sustained thrust during this narrow time window is a suitable assumption because it is on par with the propulsive period observed in extant *Nautilus* (~0.62-1.39 seconds; *Chamberlain, 1987*). While Equation 6 reports asymptotic velocities, experiments with longer durations (over larger vertical distances) are required to determine the upper velocity limit (when hydrodynamic

drag is equal to thrust). Coating the model with hydrophobic silicone yields little difference in velocity during the time window of the experiments (Fig. 5C). However, the velocity asymptote of Equation 6 between the coating and uncoated models yields a difference in 23 cm/s, suggesting that this asymptote term is very sensitive.

Modeling vertical escape maneuvers in orthocones

The time required to move one body length (t_{bl}) or half a body length ($t_{bl/2}$) under each thrust scenario was computed to determine the minimum distance (D) required to dodge a horizontally moving predator (Tables 4 and 5; Fig. 6). With higher thrust values (e.g., peak *Nautilus*-like thrust) these cephalopods could potentially thwart predator attacks from some relatively faster predators. A successful dodge, however, depends on predator maneuverability and burst swimming duration. If D is much larger than the body length of the predator, it could easily adjust its trajectory in the vertical direction and ultimately catch the relatively slower orthocone.

Discussion

The modeled ammonoid species, *Baculites compressus*, provides new context for the swimming capabilities, ecology, and adaptive value of the orthocone morphotype. Maintaining model hydrostatics in a chaotic, real-world setting demonstrates that movement is well constrained despite transient flow conditions surrounding the model (due to model rocking, minor ambient currents, and acceleration from a static initial condition; Figs. 3-5). Nuanced aspects of these properties likely varied between orthocone cephalopods with differences in ribbing intensity, whorl section shape, degree of taper, and size. Furthermore, these cephalopods likely assumed diverse life habits during their ~420 Myr intermittent range, inferred by occurrences in variable facies (*Kennedy and Cobban, 1976; Wright, Callomon, and Howarth, 1996; Kröger, Servais, and Zhang, 2009*). However, the present experiments reveal first-order constraints for the ubiquitous representatives of this persistent morphotype. Furthermore, a range of model buoyancies (thrusts) simulate possible modes of locomotion that are relevant to a broad range of orthocone taxa. The vertical movement potential revealed by the current experiments is applied further to model different scenarios involving predator evasion.

Vertical movement potential

The vertically-streamlined shape of orthocone cephalopods offers several advantages for movement in this direction. High hydrostatic stability would not have allowed these living cephalopods to considerably deviate from a vertical life habit (*Peterman et al., 2019*) unless they had sufficient counterweights to reduce stability (i.e., cameral and endosiphuncular deposits of some nautiloids; *Peterman, Barton, and Yacobucci, 2019*). When thrust is applied in the upward direction, living orthocones would have maintained a vertical orientation with negligible deviation (<8° resulting from tilted starting positions, but generally <4°; Fig. 4). The minor disturbances caused by removing the release mechanism (Fig. 3) demonstrate that slow

translation in the horizontal directions can occur from weak external currents in the water column. This behavior also suggests that horizontal thrust would only allow slow horizontal movement, which still could have been functional for the location of a mate or capture of prey items. Vertical migration, however, would have been much less expensive due to the vertical streamlining of the conch. Very low input thrust can yield high velocities relative to other ectocochleates of the same mass (Fig. 5; Tables 3 and 4). If certain orthocone cephalopods underwent similar vertical migration patterns to extant nautilids (*Ward et al., 1984; Ward, 1987; O'Dor et al., 1993; Dunstan, Ward, and Marshall, 2011*), they would require lower thrusts than those experimented upon to leisurely rise and fall in the water column. These diurnal vertical movements allow feeding at relatively shallower depths during the night to avoid predation (*Dunstan, Ward, and Marshall, 2011; Kaartvedt et al., 1996*). This feeding tactic may have been more beneficial for nautiloids in response to more abundant visual predators after the advent of the Devonian nekton revolution (*Klug et al., 2010*). For baculitids, there is evidence of both demersal behavior and somewhat higher occupation of the water column (*Tsujita and Westermann, 1998; Landman, Cobban, and Larson, 2012; Landman et al., 2018; Rowe et al., 2020)*. Perhaps these ammonoids were able to use assume either of these lifestyles, depending on the taxon or available resources. However, it should be noted that isotope values reported for *Baculites* (*Ferguson et al., 2019*) are not comparable to vertical migration ranges recorded in *Nautilus* shell material (*Linzmeier et al., 2016*).

A slightly negatively buoyant condition would be easier for the living orthocones to manage (like extant nautilids; *Ward and Martin, 1978*). The downward-facing soft body would prevent orthocones from efficiently directing a water jet upward, to counteract positive buoyancy, which may be problematic in the event of shell loss due to predation. This scenario may have been managed by ammonoid orthocones, if their complex septa improved buoyancy regulation (i.e., chamber refilling potential; *Daniel et al., 1997; Peterman et al., 2021b*). The low metabolic cost of upward movement from reduced hydrodynamic drag would apply to downward movement as well. A very small surplus in mass (~0.5 g, ~0.26% of organismal mass; *Ward and Martin, 1978*) would allow orthocones to slowly drift downwards. Without jetting, living orthocones would pick up speed (as high as 15 cm/s after 20 seconds; Fig. 5D). However, if these cephalopods were moving too fast, velocity could be managed by small, periodic jets. Furthermore, they may have been able to move in the horizontal directions or "brake" with weak jetting or simply by arranging the positions of the arms. This ability is suggested by the negatively buoyant experiments, which would start tilting toward the dorsum and moving in that direction when the downward velocity reached ~8 cm/s (Figs. 3D, 4D, 5D). This is likely due to the shape of the whorl section of *Baculites compressus*, which is thicker toward the dorsum and thinner toward the venter (similar to the cross-section of an airfoil). The position of the arms may have been able to similarly influence hydrodynamics. Sinking may have provided a low-cost feeding strategy because incident fluid would continuously move toward the mouth. The reported growth direction of a cirripede attached to the baculitid, *Sciponoceras* (*Hauschke, Schöllmann, and Keupp, 2011*) may have resulted from this direction of movement rather than

aperture-forward, horizontal swimming. For Paleozoic nautiloids, slowly sinking toward the benthos may have even qualified as a pounce, catching even slower prey items by surprise (e.g., trilobites, gastropods, other cephalopods, etc.; *Alexander, 1986; Landman and Davis, 1988; Frey, 1989; Ebbestad and Peel, 1997; Westermann, 1998; Brett and Walker, 2002; Kröger, 2004*).

Vertical escape tactics of orthocone cephalopods

During the ~420 Myr range of orthocone cephalopods, the predatory landscape significantly changed. From the Early/Middle Ordovician to the Devonian nekton revolution, large orthocones themselves were the among the dominant predators (*Brett and Walker, 2002; Kröger and Zhang, 2009; Kröger, Servais, and Zhang, 2009; Klug et al., 2010*). After this event, larger, faster, and speed-efficient nektic predators would have imposed new pressure on ectocochleate cephalopods. These changes are reflected in the evolutionary trend of increased coiling in early ammonoids, and would have continued to influence predator-prey interactions for both persisting nautiloid groups and orthocone ammonoids at different points in time. The high velocities (among ammonoids) in the experiments (Fig. 5C) suggest that vertical evasion tactics may have been feasible for some orthocones, provided that they have similar propulsive capabilities to modern *Nautilus*.

Nautiloids and ammonoids likely were eaten by other cephalopods and crustaceans throughout the Paleozoic and Mesozoic (*Landman and Waage, 1986; Klug, 2007; Kröger, Servais, and Zhang, 2009; Hoffmann et al., 2019*). After the Devonian nekton revolution began, predation of nautiloids would have intensified from durophagous and piscivorous gnathostome fishes (e.g., placoderms and sharks) due to their superior size, maneuverability, and feeding capabilities. After the Devonian mass extinction, sharks, holocephalans, and bony fishes would have served higher-tier predatory roles. Large marine reptiles (e.g., plesiosaurs, ichthyosaurs, mosasaurs, etc.) diversified and served as dominant components of marine ecosystems during the Mesozoic (*Stubbs and Benton, 2016*). Orthocone ammonoids, primarily baculitids in the Cretaceous, have well documented paleopathologies. Damage frequently occurs near the aperture at various growth stages (*Klinger and Kennedy, 2001; Kennedy, Cobban, and Klinger, 2002*), likely resulting from pycnodontid fish, coleoids (*Kennedy, Cobban, and Klinger, 2002*), and/or crustaceans (*Keupp, 2012*). Fatal injuries caused by mosasaurs are relatively common for *Baculites* as well (*Kauffman 1990; Westermann, 1996; Tsujita and Westermann, 2001*). Quick upward jetting could allow easy escape from a benthic or demersal predator (e.g., crustaceans and some cephalopods). However, thwarting attacks from the relatively quicker nektic predators would require specific escape maneuvers.

The likelihood of escape would have increased if a somewhat stationary orthocone waited to jet away from a horizontally moving predator until the last possible moment (Fig. 7A). Otherwise the predator could simply adjust its trajectory and catch up to the slower, vertically moving orthocone (Fig. 7B). Within the time it takes for an orthocone to move some percentage of its body length (100% or 50%), a successful simulated dodge occurs when the distance

between a predator (moving at its maximum velocity) and the orthocone is less than the body length of the predator (Fig. 6; Table 5). The condition was chosen because turning radius generally increases with velocity and body length (*Maresh et al., 2004*), thus reducing maneuverability and vertical correction. It should be noted that marine predators have greatly diversified in locomotor capabilities and feeding behavior through time (*Brett and Walker, 2002; Stubbs and Benton, 2016*), so this approach only represents a very general model. While this approach is simple, it suggests that orthocone cephalopods had a fighting chance of surviving the attacks of some larger predators (using extant marine predators as analogues). Larger marine predators with similar size and speed to some modern cetaceans and saltwater crocodiles may have been outmaneuvered in some cases (Table 5). However, predators with the speed and maneuverability of modern dolphins or some sharks would have been difficult to evade (Table 5). While many aspects of predation behavior are neglected in this model, it should be noted that the vertical orientation of orthocones may have made it difficult for some vertebrate predators to attack because they would have to rotate their heads ~90° to bite down on the flanks of the shell. For small, quick, highly maneuverable predators (e.g., pycnodontid fish), perhaps it was more favorable for an orthocone cephalopod to hide in its shell rather than attempting to vertically escape. Therefore, vertically escaping from larger predators that mark certain death is likely a last resort for orthocone cephalopods, which normally assume low-energy lifestyles.

Paleoecological interpretations

The low-cost vertical movement and momentarily rapid escape inferred for orthocones by the current experiments better constrain the ecology of these cephalopods. Existing morphological and ecological information can be used along with these inferred locomotive capabilities to better elucidate the life habits of these ubiquitous cephalopods.

The largely unknown soft body characteristics of orthocone cephalopods could contribute to differences in available thrust and velocities. If the propulsion of ammonoid orthocones is more similar to coleoids (*Jacobs and Landman, 1993*), closer relatives than nautiloids (*Kröger, Vinther, and Fuchs, 2011*), they may have been able to produce larger thrusts than the highest thrust value used in the current experiments (peak *Nautilus*-like thrust). However, it is unknown how confinement of the soft body in a rigid shell would reduce propulsive power compared to coleoids which can hyperinflate their mantle cavities (*Anderson and Demont, 2000*). Furthermore, the lack of well-preserved soft body material (*Klug, Riegraf, and Lehmann, 2012; Klug and Lehmann, 2015*) prevents homologization of muscles inferred by scars on the shell (*Kennedy, Cobban, and Klinger, 2002*) to the musculature of extant coleoids or nautiloids. Therefore, the thrust values in the current study pose a wide range of somewhat conservative thrust estimates for ammonoids. For orthocone nautiloids (orthocerids, endocerids, and actincocerids), muscle scars are different from those of extant *Nautilus* and tarphycerids which suggests that certain orthocone clades may have been weaker swimmers compared to coiled nautiloid clades (*Mutvei, 2002*). In this case, the *Nautilus*-like peak thrust of the current experiments may be too liberal. However, the magnitude of propulsive differences due to

differences in muscle scar size and extent are unclear in the absence of soft part preservation or modern orthocone analogues.

Exceptional preservation has been reported more commonly for baculitid ammonoids than any other orthocone (*Klug, Riegraf, and Lehmann, 2012; Klug and Lehmann, 2015*), allowing more specific interpretations of their life habit. The preservation of large putative eye capsules and the presence of lateral sinuses at their apertures suggest enhanced predator detection capabilities (*Nilsson et al., 2012*). The large ventral rostrum on many baculitid shells may have restricted thrust in the ventral direction, suggesting limited horizontal mobility. These features, along with the hydrodynamic properties inferred by the current experiments support a life habit of slowly searching for planktic prey, while maintaining the option for somewhat rapid vertical escape from large predators. For baculitids, this life habit is consistent with well-preserved mouthparts (aptychi and radulae) that support planktivory (*Landman, Larson, and Cobban, 2007; Kruta et al., 2009; Kruta et al., 2011*). A low energy lifestyle of searching for small, planktic prey can be facilitated by low-cost vertical movement or from relatively sedentary, demersal behavior (e.g., around methane seeps teeming with life; *Landman et al., 2018; Rowe et al., 2020*).

While ecological saturation (along with predatory pressure) could have stimulated increased coiling in early ammonoids (*Klug et al., 2010*), a similar saturation of planispiral forms in the Mesozoic may partially explain the iterative recurrence of orthocone ammonoids. The vertical motility of orthocone cephalopods compared to planispiral ammonoids suggests they could have occupied a distinct niche among ectocochleates. The availability of this niche may reflect suitable ecological opportunities arising from dynamic ecological conditions (e.g., predatory pressure, food resources). Similarly, dynamic environmental conditions (e.g., sea level rise, microhabitat availability; *Yacobucci, 2015*) also drive selection and speciation in ammonoids, which may have increased the availability of this niche in newly-formed epeiric seas. Our results offer interpretations for the adaptive value of orthocone cephalopods and potential drivers behind their iterative recurrence in the fossil record.

Conclusions

The high hydrostatic stability of orthocone cephalopods without cameral deposits (*Peterman et al., 2019; Peterman, Barton, and Yacobucci, 2019*) would have strictly constrained the life habits of these animals. They would have been confined to vertical orientations without the capacity to substantially modify them. These properties raise questions about the modes of life, functional morphology, and adaptive value of the orthocone morphotype. The hydrodynamics inferred by 3D-printed models of the baculitid, *Baculites compressus*, suggest that vertical movement was well constrained for orthocones (Figs. 3 and 5). High hydrostatic stability prevents rocking during movement, even with somewhat variable starting angles (Fig. 4). High velocities relative to other ectocochleates of similar size suggests that low hydrodynamic drag is incurred by movement in the upwards direction. Therefore, these living cephalopods required very low energy to vertically migrate in the water column (probably at

554 velocities lower than those in the current study; Fig. 5). Slight negative buoyancy (like extant
555 nautilids, *Ward and Martin, 1978*) would have allowed these cephalopods do slowly sink after
556 jet thrust is suspended. This would have allowed low-energy movement and feeding for vertical
557 migrants. For early nautiloids, this condition would have allowed them to pounce on benthic prey
558 from above. While these cephalopods likely assumed low energy lifestyles, *Nautilus*-like peak
559 thrust would have given orthocones a fighting chance at vertically escaping attacks by larger
560 predators. While coiled ectocochleate cephalopods flourished from the Devonian to end of the
561 Cretaceous, orthocone cephalopods retained adaptive value during this time as low-energy
562 vertical migrants and periodic escape artists.
563

564 ## Acknowledgements

565 We appreciate the help of Emma Janusz and Mark Weiss for accommodating our experiments at
566 the University of Utah pool (the Crimson Lagoon).
567

568 ## References

569 Alexander RR. 1986. Resistance to and repair of shell breakage induced by durophages in Late
570 Ordovician brachiopods. Journal of Paleontology 60: 273–285.
571 Anderson EJ, Demont ME. 2000. The mechanics of locomotion in the squid *Loligo pealei*:
572 locomotory function and unsteady hydrodynamics of the jet and intramantle pressure. The
573 Journal of Experimental Biology 203: 2851–2863.
574 Anderson EJ, Grosenbaugh MA. 2005. Jet flow in steadily swimming adult squid. Journal of
575 Experimental Biology 208: 1124–1146d. DOI 10.1242/jeb.01507.
576 Benga G, Chapman BE, Cox GC, Kuchel PW. 2010. Comparative NMR studies of diffusional
577 water permeability of red blood cells from different species: XVIII platypus
578 (*Ornithorhynchus anatinus*) and saltwater crocodile (*Crocodylus porosus*). Cell Biology
579 International 34: 703–708. DOI 10.1042/CBI20090430.
580 Blender Online Community. 2017. Blender, a 3D modelling and rendering package. Blender
581 Institute, Amsterdam. Available at: http://www.blender.org. Accessed 1 June 2018.
582 Brett C, Walker S. 2002. Predators and predation in Paleozoic marine environments.
583 Paleontological Society Papers 8: 93–118.
584 Chamberlain Jr. JA. 1987. Locomotion in *Nautilus*. In: Saunders, W.B., Landman, N.H., eds.
585 *Nautilus*—the biology and paleobiology of a living fossils. Springer, Dordrecht, 489–526.
586 Cignoni P, Ranzuglia G. 2014. MeshLab. Version 1.3.3. Visual Computing Lab, Pisa, Italy.
587 Available from: http://meshlab.sourceforge.net/. Accessed 1 August 2018.
588 Daniel TL, Helmuth BS, Saunders WB, Ward PD. 1997. Septal complexity in ammonoid
589 cephalopods increased mechanical risk and limited depth. Paleobiology 23: 470–481.
590 Dunstan AJ, Ward PD, and Marshall NJ. 2011. Vertical distribution and migration patterns of
591 *Nautilus pompilius*. PLoS ONE 6: e16311. DOI 10.1371/journal.pone.0016311.
592 Ebbestad JOR, Peel JS. 1997. Attempted predation and shell repair in Middle and Upper
593 Ordovician gastropods from Sweden. Journal of Paleontology 71: 1047–1060.

Erben HK. 1996. Über den Ürsprung der Ammonoidea. Biological Reviews 41: 641–658. DOI 10.1111/j.1469-185X.1966.tb01626.x.

Fatherree JW, Harries PJ, Quinn TM. 1998. Oxygen and carbon isotopic “dissection” of *Baculites compressus* (Mollusca: Cephalopoda) from Pierre Shale (Upper Campanian) of South Dakota: implications for paleoenvironmental reconstructions. Palaios 13: 376–385.

Ferguson K, MacLeod KG, Landman NH, Sessa JA. 2019. Evaluating growth and ecology in baculitid and scaphitid ammonites using stable isotope sclerochronology. Palaios 34: 317–329. DOI 10.2110/palo.2019.005.

Fernandez-Waid P, Diez G, Bidaguren I, Izagirre U, Blanco JM, Soto M. 2019. Morphological characterization of hydrodynamic behavior of shortfin mako shark (*Isurus oxyrinchus*) dorsal fin denticles. Journal of Bionic Engineering 16: 730–741. DOI 10.1007/s42235-019-0059-7.

Flower RH. 1955. Trails and tentacular impressions of orthoconic cephalopods. Journal of Paleontology 29: 857–867.

Frey RC. 1989. Paleoecology of well-preserved nautiloid assemblages from a Late Ordovician shale unit, south-west Ohio. Journal of Paleontology 63: 604–620.

Hauschke N, Schöllmann L, Keupp H. 2011. Oriented attachment of a stalked cirripede on an orthoconic heteromorph ammonite—implications for the swimming position of the latter. Neues Jahrbuch für Geologie und Paläontologie Abhandlungen 202: 199–212. DOI 10.1127/0077-7749/2011/0192.

Hedrick TL. 2008. Software techniques for two- and three- dimensional kinematic measurements of biological and biomimetic systems. Bioinspiration and biomimetics 3: 034001. DOI 10.1088/1748-3182/3/3/034001.

Henderson RA, Price GD. 2012. Paleoenvironment and paleoecology inferred from oxygen and carbon isotopes of subtropical mollusks from the late Cretaceous (Cenomanian) of Bathurst Island, Australia. Palaios 27: 617–626. DOI 10.2110/palo.2011.p11-120r.

Hoffmann R, Lemanis R, Naglik C, Klug C. 2015. Ammonoid buoyancy. In: Klug C, Korn D, De Baets K, Kruta I, Mapes RH, eds. Ammonoid Paleobiology: from anatomy to ecology. Topics in Geobiology 44, Springer, Dordrecht. 613–648. DOI 10.1007/978-94-017-9630-9_16.

Hoffmann R, Stevens K, Keupp H, Simonsen S, Schweigert G. 2019. Regurgitalites – a window into the trophic ecology of fossil cephalopods. Journal of the Geological Society 177: 82–102. DOI 10.1144/jgs2019-177.

Hoffmann R, Slattery JS, Kruta I, Linzmeier BJ, Lemanis RE, Mironenko A, Goolaerts S, De Baets K, Peterman DJ, Klug C. 2021. Recent advances in heteromorph ammonoid paleobiology. Biological Reviews 96: 576–610. DOI 10.1111/brv.12669.

Kaartvedt S, Melle W, Knutsen T, Skjoldal HR. 1996. Vertical distribution of fish and krill beneath water of varying optical properties. Marine Ecology Progress Series 136: 51–58.

Kauffman EG. 1990. Mosasaur predation on ammonites during the Cretaceous-an evolutionary history. In: Boucot AJ, ed., Evolutionary paleobiology of behavior and coevolution. Elsevier, New York. 184–189.

Kennedy WJ, Cobban WA. 1976. Aspects of ammonite biology, biogeography, and biostratigraphy. Special Papers in Palaeontology No. 17: 94p.

Kennedy WJ, Cobban WA, Klinger HC. 2002. Muscle attachment and mantle-related features in Upper Cretaceous *Baculites* from the United States Western Interior. Abhandlungen der Geologischen Bundesantstalt Wien 57: 89–112.

Keupp H. 2012. Atlas zur Paläopathologie der Cephalopoden. Berliner paläobiologische Abhandlungen 12: 1–392.

Klinger HC, Kennedy WJ. 2001. Stratigraphic and geographic distribution, phylogenetic trends and general comments on the ammonite family Baculitidae Gill, 1871 (with an annotated list of species referred to the family). Annals of the South African Museum 107: 1–29.

Klug C. 2007. Sublethal injuries in early Devonian cephalopod shells from Morocco. Ata Palaeontologica Polonica 52: 749–759.

Klug C, Korn D. 2004. The origin of ammonoid locomotion. Acta Palaeontologica Polonica 49: 235–242.

Klug C, Kröger B, Kiessling W, Mullins GL, Servais T, Frýda J, Korn D, Turner S. 2010. The Devonian nekton revolution. Lethaia 43: 465–477.

Klug C, Lehmann J. 2015. Soft part anatomy of ammonoids: reconstructing the animal based on exceptionally preserved specimens and actualistic comparisons. In: Klug C, Korn D, De Baets K, Kruta I, Mapes RH, eds., Ammonoid paleobiology: from anatomy to ecology: Topics in Geobiology 44, Springer, Dordrecht. 515–538. DOI 10.1007/978-94-017-9630-9_12.

Klug C, Riegraf W, Lehmann J. 2012. Soft-part preservation in heteromorph ammonites from the Cenomanian-Turonian Boundary Even (OAE 2) in the Teutoburger Wald (Germany). Palaeontology 55: 1307–1331.

Kröger B. 2004. Large shell injuries in Middle Ordovician Orthocerida (Nautiloidea, Cephalopoda). GFF 126: 311–316.

Kröger B, Mapes RH. 2007. On the origin of bactritoids (Cephalopoda). Paläontologische Zeitschrift 81: 316–327.

Kröger B, Zang Y. 2009. Pulsed cephalopod diversification during the Ordovician. Palaeogeography, Palaeoclimatology, Palaeoecology 273: 174–183. DOI 10.1016/j.palaeo.2008.12.015.

Kröger B, Servais T, Zhang Y. 2009. The origin and initial rise of pelagic cephalopods in the Ordovician. PLoS ONE 4: e7262. doi:10.1371/journal.pone.0007262.

Kröger B, Vinther J, Fuchs D. 2011. Cephalopod origin and evolution: a congruent picture emerging from fossils, development and molecules. Bioessays 33: 602–613. DOI 10.1002/bies.201100001.

Kruta I, Rouget I, Landman NH, Tanabe K, Cecca F. 2009. Aptychus microstructure in Late Cretaceous Ancyloceratina (Ammonoidea). Lethaia 42: 312–321. DOI 10.1111/j.1502-3931.2009.00154.x.

673 Kruta I, Landman N, Rouget I, Cecca F, Tafforeau P. 2011. The role of ammonites in the
674 Mesozoic marine food web revealed by jaw preservation. Science 331: 70–72. DOI
675 10.1126/science.1198793.
676 Landman NH. 1982. Embryonic shells of *Baculites*. Journal of Paleontology 56: 1235–1241.
677 Landman NH, Waage KM. 1986. Shell abnormalities in scaphitid ammonites. Lethaia 19: 211–
678 224.
679 Landman NH, Davis RA. 1988. Jaw and crop in an orthoconic nautiloid from the Bear Gulch
680 Limestone (Mississippian, Montana). Memoir – New Mexico Bureau of Mines and Mineral
681 Resources 44: 103–107.
682 Landman NH, Larson NL, Cobban WA. 2007. Jaws and radula of *Baculites* from the Upper
683 cretaceous (Campanian) of North America. In: Landman NH, Davis RA, Mapes RH, eds.,
684 Cephalopods present and past: new insights and fresh perspectives. Springer, Dordrecht.
685 257–298.
686 Landman NH, Cobban WA, Larson NL. 2012. Mode of life and habitat of scaphitid ammonites.
687 Geobios 45: 87–98. DOI 10.1016/j.geobios.2011.11.006.
688 Landman NH, Cochran JK, Sovacek M, Larson NL, Garb MP, Brezina J, Witts JD. 2018.
689 Isotope sclerochronology of ammonites (*Baculites compressus*) from methane seep and non-
690 seep sites in the Late Cretaceous Western Interior Seaway, USA: Implications for ammonite
691 habitat and mode of life. American Journal of Science 318: 603–639. DOI
692 10.2475/06.2018.01.
693 Lindgren J, Caldwell MW, Konishi T, Chiappe LM. 2010. Convergent evolution in aquatic
694 tetrapods: insights from an exceptional fossil mosasaur. PLoS ONE 5:e11998. DOI
695 10.1371/journal.pone.0011998.
696 Linzmeier BJ, Kozdon R, Peters SE, Valley JW. 2016. Oxygen isotope variability within
697 *Nautilus* shell growth bands. PLoS ONE 11: e0153890. DOI 10.1371/journal.pone.0153890.
698 Lukeneder A. 2015. Ammonoid habitats and life history. In: Klug C, Korn D, De Baets K, Kruta
699 I, Mapes RH, eds. Ammonoid Paleobiology: from macroevolution to paleogeography. Topics
700 in Geobiology 44, Springer, Dordrecht. 689–791. DOI 10.1007/978-94-017-9630-9_18.
701 Lukeneder A, Harzhauser M, Müllegger S, Piller WE. 2010. Ontogeny and habitat change in
702 Mesozoic cephalopods revealed by stable isotopes ($\delta^{18}O$, $\delta^{13}C$). Earth and Planetary Science
703 296: 103–114. DOI 10.1016/j.epsl.2010.04.053.
704 Manda S, Turek V. 2015. Colour patterns on Silurian orthocerid and pseudorthocerid conchs
705 from Gotland – palaeoecological implications. Estonian Journal of Earth Sciences 64: 74–79.
706 DOI 10.3176/earth.2015.13.
707 Maresh JL, Fish FE, Nowacek DP, Nowacek SM. 2004. High performance turning capabilities
708 during foraging by bottlenose dolphins (Tursiops truncatus). Marine Mammal Science 20:
709 498–509.
710 Monnet C, De Baets K, Klug C. 2011. Parallel evolution controlled by adaptation and
711 covariation in ammonoid cephalopods. BMC Evolutionary Biology 11: 1–21. DOI
712 10.1186/1471-2148-11-115.

Monnet C, Klug C, De Baets K. 2015. Evolutionary patterns of ammonoids: phenotypic trends, convergence, and parallel evolution. In: Klug C, Korn D, De Baets K, Kruta I, Mapes RH, eds. Ammonoid Paleobiology: from macroevolution to paleogeography. Topics in Geobiology 44, Springer, Dordrecht. 95–142. DOI 10.1007/978-94-017-9633-0_5.

Motani R. 2002. Swimming speed estimation of extinct marine reptiles: energetic approach revisited. Paleobiology 28: 251–262.

Mutvei H. 2002. Connecting ring structure and its significance for classification of the orthocerid cephalopods. Acta Palaeontologica Polonica 47: 157–168.

Neil TR, Askew GN. 2018. Swimming mechanics and propulsive efficiency in the chambered nautilus. Royal Society Open Science 5: 170467. DOI 10.1098/rsoc.170467.

Nilsson DE, Warrant EJ, Johnsen S, Hanlon R, Shashar N. 2012. A unique advantage for giant eyes in giant squid. Current Biology 22: 683–688. DOI 10.1016/j.cub.2012.02.031.

O'Dor RK, Forsythe J, Webber DM, Wells J, Wells MJ. 1993. Activity levels of *Nautilus* in the wild. Nature 362: 626–628.

Packard A. 1988. Visual tactics and evolutionary strategies. In: Wiedmann J, Kullmann J, eds., Cephalopods – Present and Past. Schweizerbart'sche, Stuttgart. 89–103.

Peterman DJ, Ciampaglio C, Shell RC, Yacobucci MM. 2019. Mode of life and hydrostatic stability of orthoconic ectocochleate cephalopods: hydrodynamic analyses of restoring moments from 3D-printed, neutrally buoyant models of a baculite. Acta Palaeontologica Polonica 64: 441–460. DOI 10.4202/app.00595.2019.

Peterman DJ, Barton CC, Yacobucci MM. 2019. The hydrostatics of Paleozoic ectocochleate cephalopods (Nautiloidea and Endoceratoidea) with implications for modes of life and early colonization of the pelagic zone. Palaeontologia Electronica 22.2.27A: 1–29. DOI 10.26879/884.

Peterman DJ, Hebdon N., Ciampaglio CN, Yacobucci MM, Landman NH, Linn T. 2020a. Syn vivo hydrostatic and hydrodynamic properties of scaphitid ammonoids from the U.S. Western Interior. Geobios 60: 79–98. DOI 10.1016/j.geobios.2020.04.004.

Peterman DJ, Shell RC, Ciampaglio CN, Yacobucci MM. 2020b. Sable hooks: biomechanics of heteromorph ammonoids with U-shaped body chambers. Journal of Molluscan Studies 86: 267–279. DOI 10.1093/mollus/eyaa018.

Peterman DJ, Hebdon N, Shell RC, Ritterbush A. 2021a. Twirling torticones: hydrostatics and hydrodynamics of helically-coiled ammonoids. In: Slattery JS, Larson NL, Bingle-Davis M., eds. Insights into the Cretaceous: Building on the Legacy of William A. Cobban (1916-2015), Wyoming Geological Association Special Volume, forthcoming.

Peterman DJ, Ritterbush KA, Ciampaglio CN, Johnson EH, Inoue S, Mikami T, Linn TJ. 2021b. Complex shell architecture refined buoyancy control in ammonoid cephalopods. Scientific Reports 11: 8055. DOI 10.1038/s41598-021-87379-5.

Rowe AJ, Landman NH, Cochran JK, Witts JD, Garb MP. 2020. Late Cretaceous methane seeps as habitats for newly hatched ammonites. Palaios 35: 151–163. DOI 10.2110/palo.2019.105.

Segre PS, Potvin J, Cade DE, Calambokidis J, Clemente JD, Fish FE, Fridlaender AS, Gough WT, Kahane-Rapport SR, Oliveira C, Parks SE, Penry GS, Simon M, Stimpert AK, Wiley DN, Bierlich KC, Madsen PT, Goldbogen JA. 2020. Energetic and physical limitations on the breaching performance of large whales. eLife 9: e51760. DOI 10.7554/eLife.51760.

Sessa JA, Larina E, Knoll K, Garb M, Cochran JK, Huber BT, MacLeod KG, Landman NH. 2015. Ammonite habitat revealed via isotopic composition and comparisons with co-occurring benthic and planktonic organisms. PNAS 112: 15562–15567. DOI 10.1073/pnas.1507554112.

Tanaka H, Li G, Uchida Y, Nakamura M, Ikeda T, Liu H. 2019. Measurement of time-varying kinematics of a dolphin in burst accelerating swimming. PLoS ONE 14: e0210860. DOI 10.1371/journal.pone.0210860.

Teichert C, Kummel B, Sweet WC, Stenzel HB, Furnish WM, Glenister BF, Erben HK, Moore RC, Zeller DE. 1964. Part K, Mollusca 3, Cephalopoda – General Features, Endoceratoidea, Actinoceratoidea, Nautiloidea, Bactritoidea. In: Moore, R.C., ed. Treatise on Invertebrate Paleontology. Geological Society of America and The University of Kansas Press, Boulder. 519p.

Theriault DH, Fuller NW, Jackson BE, Bluhm E, Evangelista D, Wu Z, Betke M, Hedrick TL. 2014. A protocol and calibration method for accurate multi-camera field videography. The Journal of Experimental Biology 217: 1843–1848. DOI 10.1242/jeb.100529.

Trueman AE. 1941. The ammonite body chamber, with special reference to the buoyancy and mode of life of the living ammonite. Quarterly Journal of the Geological Society 384: 339–383.

Tsujita CJ, Westermann GEG. 1998. Ammonoid habitats and habits in the Western Interior Seaway: a case study from the Upper Cretaceous Bearpaw Formation of southern Alberta, Canada. Palaeogeography, Palaeoclimatology, Palaeoecology 144: 135–160.

Tsujita CJ, Westermann GEG. 2001. Were limpets or mosasaurs responsible for perforations in the ammonite *Placenticeras*? Palaeogeography, Palaeoclimatology, Palaeoecology 169: 245–270.

Ward PD, Martin A. 1978. On the buoyancy of the Pearly *Nautilus*. Journal of Experimental Zoology 205: 5–12. DOI 10.1002/jez.1402050103

Ward PD. 1987. The natural history of *Nautilus*. Allen and Unwin, Winchester. 267 p.

Ward PD, Carlson B, Weekly M, Brumbaugh B. 1984. Remote telemetry of daily vertical and horizontal movement of *Nautilus* in Palau. Nature 309: 248–250.

Webber DM, O'Dor RK. 1986. Monitoring the metabolic rate and activity of free-swimming squid with telemetered jet pressure. Journal of Experimental Biology 126: 205–224.

Wells MJ, O'Dor RK. 1991. Jet propulsion and the evolution of the cephalopods. Bulletin of Marine Science 49: 419–432.

Westermann GEG. 1977. Form and function of orthocone cephalopod shells with concave septa. Paleobiology 3: 300–321.

Westermann GEG. 1996. Ammonoid life and habitat. In: Landman NH, Tabane K, Davis RA, eds., Ammonoid Paleobiology. Plenum, New York. 607–707.
Westermann GEG. 1998. Life habits of nautiloids. In: Savazzi, ed., Functional Morphology of the Invertebrate Skeleton. John Wiley & Sons, Chichester, New York. 263–298.
Wiedmann J. 1969. The heteromorphs and ammonoid extinction. Biological Reviews 44: 463–602.
Wright CW, Callomon JH, Howarth MK. 1996. Part L Mollusca 4 Revised, Vol. 4: Cretaceous Ammonoidea. In: Moore, R.C., ed. Treatise on Invertebrate Paleontology. Geological Society of America and The University of Kansas Press, Boulder. 362 p.
Yacobucci MM. 2015. Macroevolution and Paleobiogeography of Jurassic-Cretaceous Ammonoids. In: Klug C, Korn D, De Baets K, Kruta I, Mapes RH, eds. Ammonoid Paleobiology: from macroevolution to paleogeography. Topics in Geobiology 44, Springer, Dordrecht. 189–228.

Figure and Table Captions

Figure 1: Construction of a physical, 3D-printed model of *Baculites compressus* from a virtual hydrostatic model. A) Virtual model used to determine hydrostatic properties (modified from *Peterman et al., 2019*). B) Virtual model with simplified internal geometry that allows for 3D printing. The total model mass was manipulated to impart an upward buoyant force, simulating downward thrust. The total center of mass (m) relative to the center of buoyancy (b) was maintained with an adorally placed counterweight and various internal voids. C) Physical, 3D-printed model with tracking points placed at the distal ends of the arms and apex used for 3D motion tracking.

Figure 2: Underwater camera rig used for 3D motion tracking. A) Schematic of the camera rig relative to the model (yellow) and release mechanism (green). The rig was made strongly negatively buoyant with three steel counterweights at the ends (purple). The wireframe shapes radiating from the cameras denote the approximate field of view. B) Close-up view of waterproof camera and LED light with custom, 3D-printed attachments.

Figure 3: Three-dimensional positions from a common starting point for each model through time. A) Scenario 1: *Nautilus*-like cruising thrust. B) Scenario 2: *Nautilus*-like cruising thrust scaled by the higher mantle cavity ratio of *Sepia*. C) Scenario 3: *Nautilus*-like peak thrust. D) Scenario 4: slightly negatively buoyant (~0.26% of mass not relieved by buoyancy).

Figure 4: Maximum displacement angle in any direction from the vertical axis through time. Each trial is distinguished by color. A) Scenario 1: *Nautilus*-like cruising thrust. B) Scenario 2: *Nautilus*-like cruising thrust scaled by the higher mantle cavity ratio of *Sepia*. C) Scenario 3:

Nautilus-like peak thrust. D) Scenario 4: slightly negatively buoyant (~0.26% of mass not relieved by buoyancy).

Figure 5: Velocity in the direction of movement as a function of time. All trials are fit with an asymptote equation. A) Scenario 1: *Nautilus*-like cruising thrust. B) Scenario 2: *Nautilus*-like cruising thrust scaled by the higher mantle cavity ratio of *Sepia*. C) Scenario 3: *Nautilus*-like peak thrust. A hydrophobic coating was applied to the original model to compare the influence of surface texture and friction drag. D) Scenario 4: slightly negatively buoyant (~0.26% of mass not relieved by buoyancy).

Figure 6: Diagram of vertical predator escape and related terms. The time required to move one body length (t_{bl}) or half a body length ($t_{bl/2}$) was computed for each velocity profile (V; Fig. 5). This time was multiplied by the velocity of various predators (V_p) to compute the minimum distance required to start jetting (D). A dodge was considered successful if D is less than the length of the predator (L_p). The image of the mosasaur (*Platecarpus*) was created from the outline inferred by *Lindgren et al. (2010)*.

Figure 7: Scenarios involving successful dodging (A) and unsuccessful dodging (B). The cruising predator first notices the prey (i), then begins to accelerate (ii). After closing in (iii), the predator makes its final lunge for the prey (iv). Cones surrounding the predator indicate hypothetical turning radiuses. For a successful dodge, the orthocone cephalopod must wait until the last possible moment or else the incoming predator could adjust its vertical trajectory. The image of the mosasaur (*Platecarpus*) was created from the outline inferred by *Lindgren et al. (2010)*.

Table 1: Local centers of mass for the model components (PLA plastic and bismuth counterweight), and total centers of mass and buoyancy for each model (1: *Nautilus*-like cruising thrust; 2: *Nautilus*-like cruising thrust scaled by the higher mantle cavity ratio of *Sepia*; 3: *Nautilus*-like peak thrust; 4: Slightly negatively buoyant). Only the x and z values are reported because the virtual model is perfectly symmetrical. All coordinates are measured relative to the same arbitrary datum (located in the center of the aperture).

.

Table 2: Masses (m) and volumes (V) for the virtual and physical model components. 1: *Nautilus*-like cruising thrust; 2: *Nautilus*-like cruising thrust scaled by the higher mantle cavity ratio of *Sepia*; 3: *Nautilus*-like peak thrust; 4: Slightly negatively buoyant. PLA = 3D printed plastic; Bi = bismuth counterweight; wd = water displaced; Mass def. = mass deficiency required to impart the computed buoyant forces (Table 3); glue = the cyanoacrylate glue used to secure each counterweight. The residual mass in the negatively buoyant experiment (denoted with *) was not weighed, but rather its volume was inserted into the model with a syringe (~0.5 cm^3).

Table 3: Virtual and actual hydrostatic stabilities (S_t) and thrusts (F), and computed percent errors. 1: *Nautilus*-like cruising thrust; 2: *Nautilus*-like cruising thrust scaled by the higher mantle cavity ratio of *Sepia*; 3: *Nautilus*-like peak thrust; 4: Slightly negatively buoyant.

Table 4: Velocities, travel times, and asymptote equation coefficients. Uncertainty reflects bounds of 95% confidence intervals. The asymptotic velocity (in cm/s) is predicted by coefficient "a" of Equation 6. Coefficient "b" governs the slope. The maximum body lengths per second (Max. bl/s) were computed by dividing velocity by the body length of the models (57 cm). The time required to move one body length (t_{bl}) and half of one body length ($t_{bl/2}$) was computed for each model (1: *Nautilus*-like cruising thrust; 2: *Nautilus*-like cruising thrust scaled by the higher mantle cavity ratio of *Sepia*; 3: *Nautilus*-like peak thrust, coated and uncoated with hydrophobic silicone spray).

Table 5: Predator evasion potential of orthocone cephalopods using mostly extant predators as analogues. Dodges are considered successful (highlighted green) when the minimum distance required to start jetting (D) is less than the body length of a predator (L_p) moving at some incident velocity (V_p). The subscripts in D values refer to different thrust scenarios in the models (1: *Nautilus*-like cruising thrust; 2: *Nautilus*-like cruising thrust scaled by the higher mantle cavity ratio of *Sepia*; 3uc: *Nautilus*-like peak thrust with no coating; 3c: *Nautilus*-like peak thrust, coated in hydrophobic silicone spray). The velocity of *Platecarpus* (denoted by *) is only an estimate of metabolically optimal velocity (*Motani, 2002*), therefore critical/lunge velocity should be much higher.

Figure 1

Construction of a physical, 3D-printed model of *Baculites compressus* from a virtual hydrostatic model.

A) Virtual model used to determine hydrostatic properties (modified from *Peterman et al., 2019*). B) Virtual model with simplified internal geometry that allows for 3D printing. The total model mass was manipulated to impart an upward buoyant force, simulating downward thrust. The total center of mass (m) relative to the center of buoyancy (b) was maintained with an adorally placed counterweight and various internal voids. C) Physical, 3D-printed model with tracking points placed at the distal ends of the arms and apex used for 3D motion tracking.

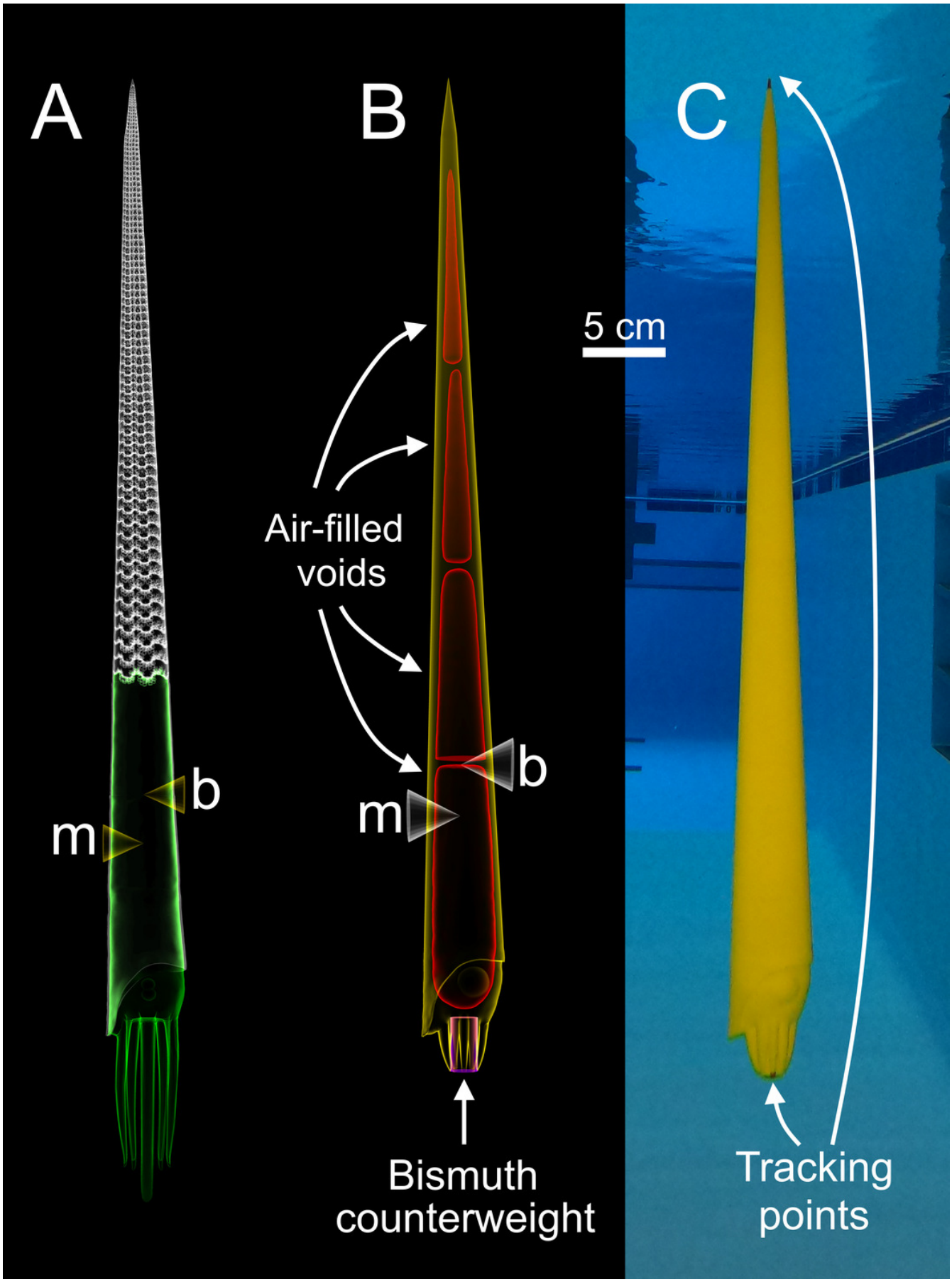
A
B
C
5 cm
Air-filled
voids
b
m
b
m
Bismuth
counterweight
Tracking
points

Figure 2

Underwater camera rig used for 3D motion tracking.

A) Schematic of the camera rig relative to the model (yellow) and release mechanism (green). The rig was made strongly negatively buoyant with three steel counterweights at the ends (purple). The wireframe shapes radiating from the cameras denote the approximate field of view. B) Close-up view of waterproof camera and LED light with custom, 3D-printed attachments.

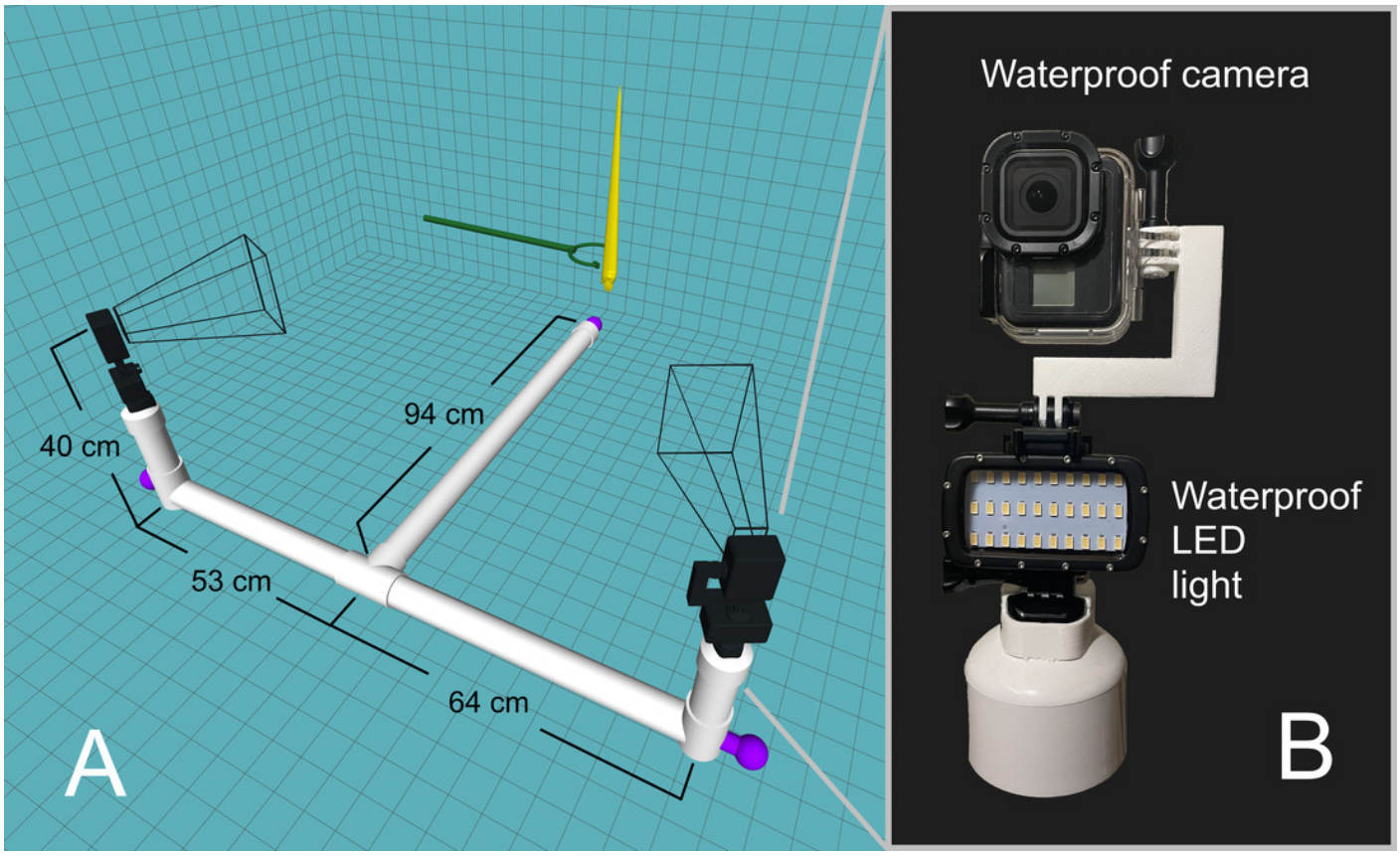

Figure 3

Three-dimensional positions from a common starting point for each model through time.

A) Scenario 1: *Nautilus*-like cruising thrust. B) Scenario 2: *Nautilus*-like cruising thrust scaled by the higher mantle cavity ratio of *Sepia*. C) Scenario 3: *Nautilus*-like peak thrust. D) Scenario 4: slightly negatively buoyant (~0.26% of mass not relieved by buoyancy).

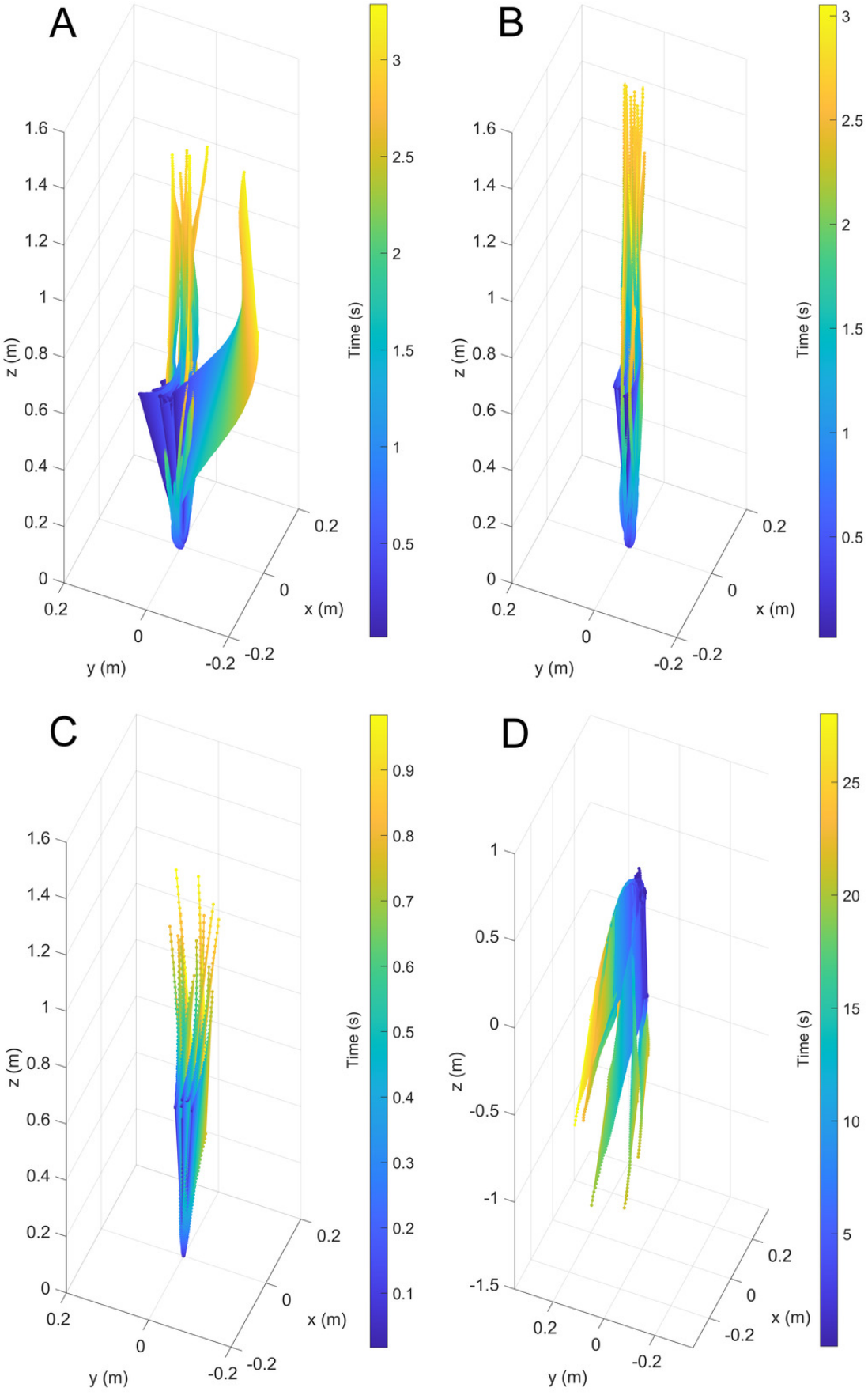
A
B
C
D
z (m)
y (m)
x (m)
Time (s)

Figure 4

Maximum displacement angle in any direction from the vertical axis through time.

Each trial is distinguished by color. A) Scenario 1: *Nautilus*-like cruising thrust. B) Scenario 2: *Nautilus*-like cruising thrust scaled by the higher mantle cavity ratio of *Sepia*. C) Scenario 3: *Nautilus*-like peak thrust. D) Scenario 4: slightly negatively buoyant (~0.26% of mass not relieved by buoyancy).

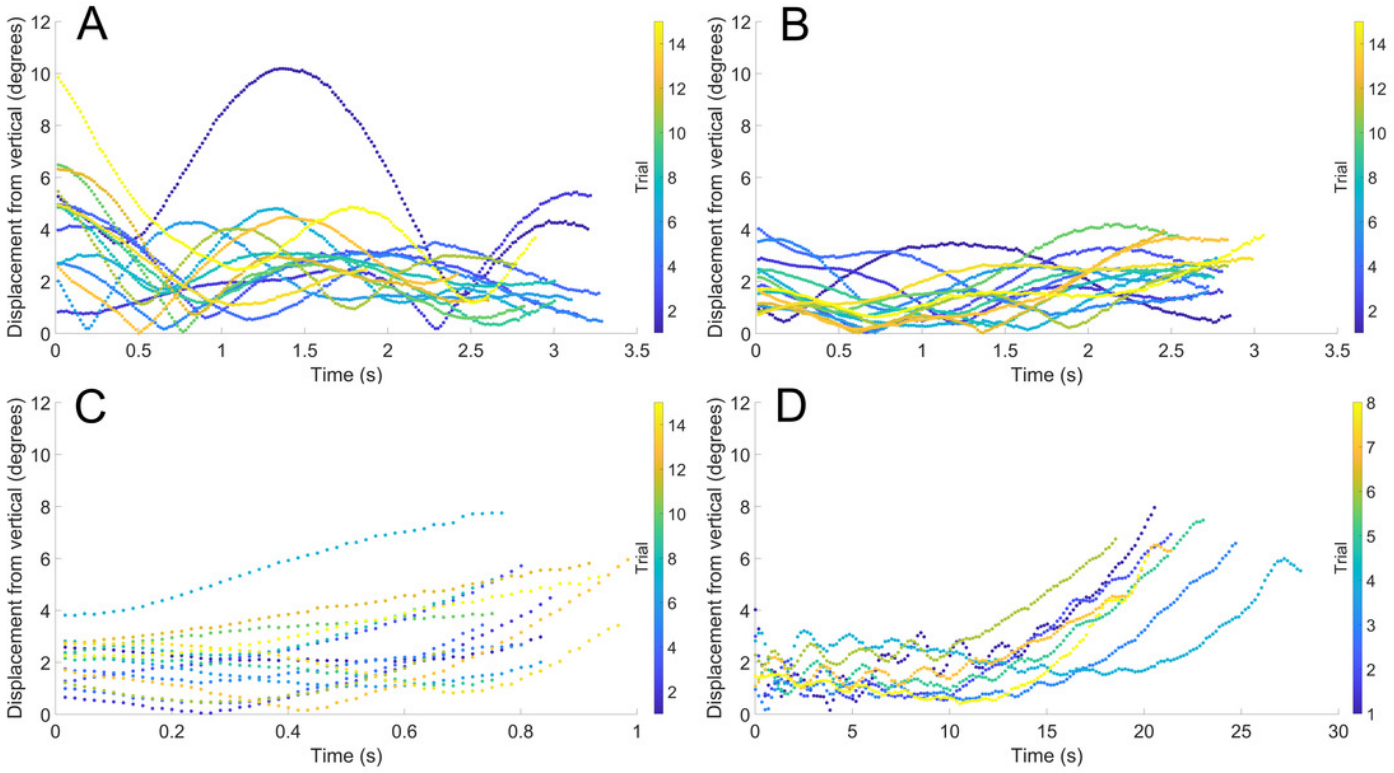

Figure 5

Velocity in the direction of movement as a function of time.

All trials are fit with an asymptote equation. A) Scenario 1: *Nautilus*-like cruising thrust. B) Scenario 2: *Nautilus*-like cruising thrust scaled by the higher mantle cavity ratio of *Sepia*. C) Scenario 3: *Nautilus*-like peak thrust. A hydrophobic coating was applied to the original model to compare the influence of surface texture and friction drag. D) Scenario 4: slightly negatively buoyant (~0.26% of mass not relieved by buoyancy).

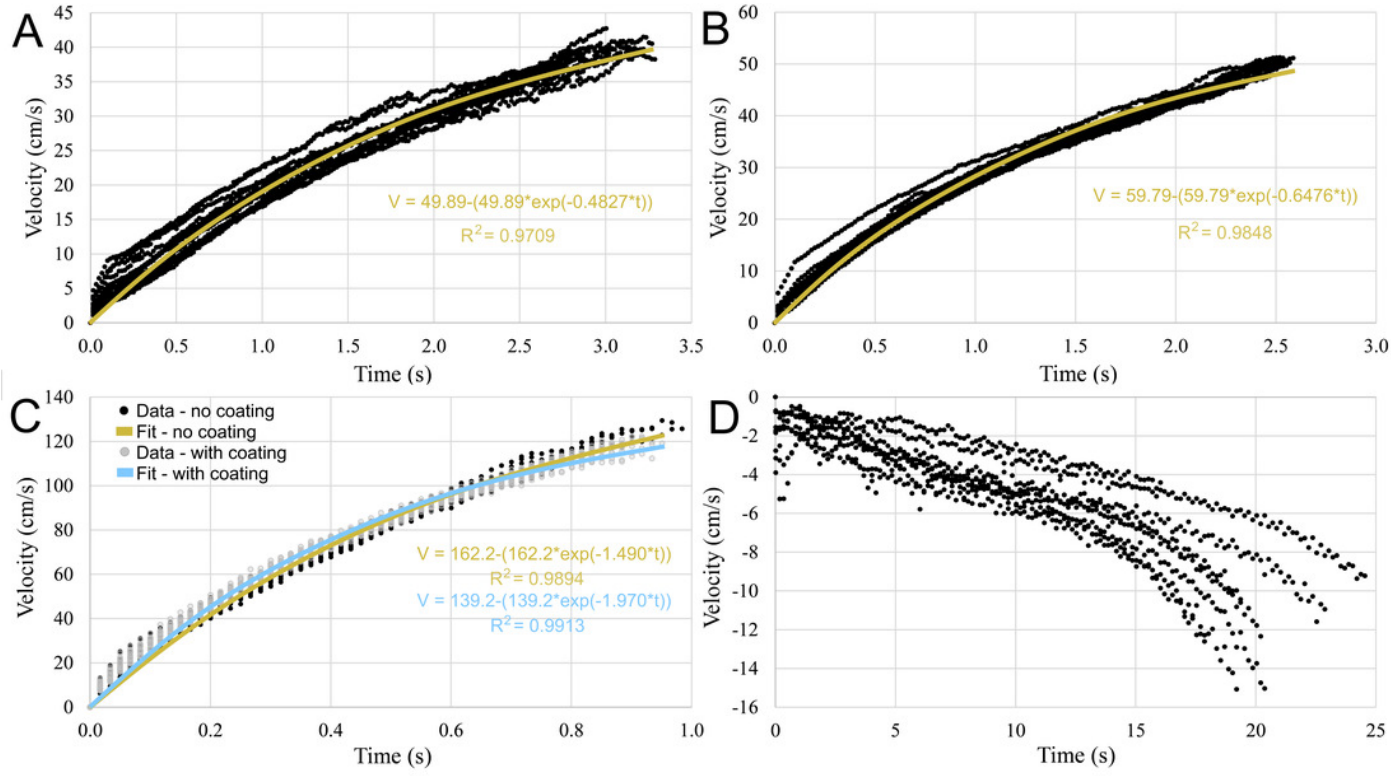

Figure 6

Diagram of vertical predator escape and related terms.

The time required to move one body length (t_{bl}) or half a body length ($t_{bl/2}$) was computed for each velocity profile (V; Fig. 5). This time was multiplied by the velocity of various predators (V_p) to compute the minimum distance required to start jetting (D). A dodge was considered successful if D is less than the length of the predator (L_p). The image of the mosasaur (*Platecarpus*) was created from the outline inferred by *Lindgren et al. (2010)*.

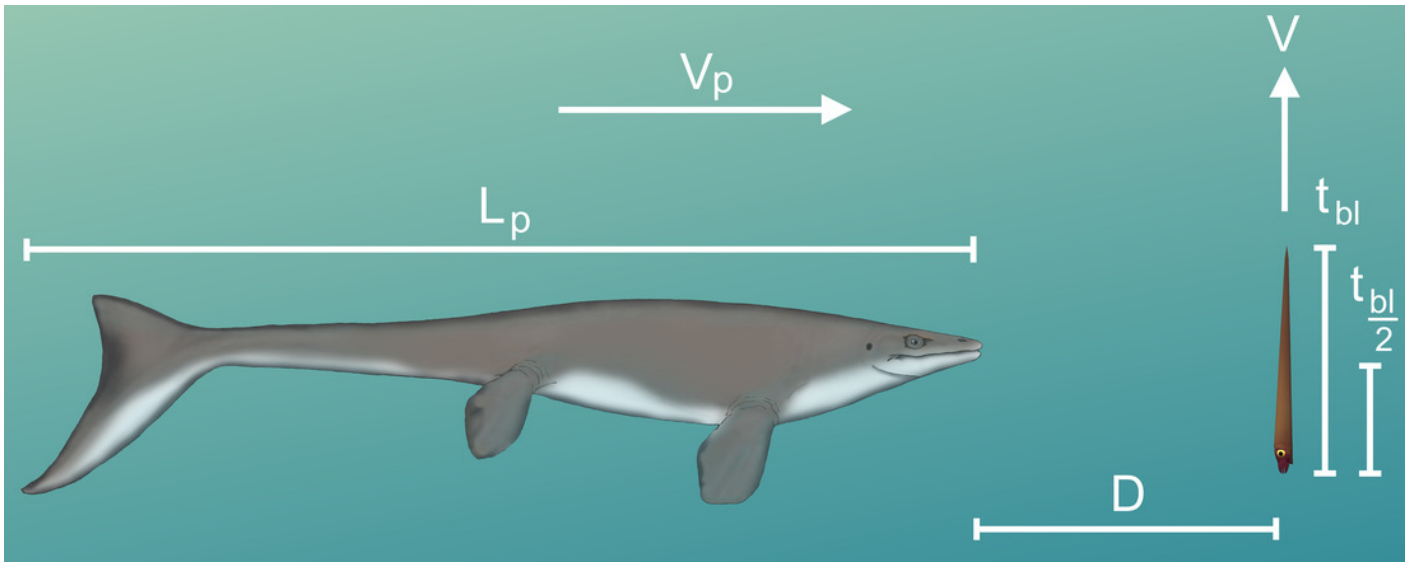

Figure 7

Scenarios involving successful dodging (A) and unsuccessful dodging (B).

The cruising predator first notices the prey (i), then begins to accelerate (ii). After closing in (iii), the predator makes its final lunge for the prey (iv). Cones surrounding the predator indicate hypothetical turning radiuses. For a successful dodge, the orthocone cephalopod must wait until the last possible moment or else the incoming predator could adjust its vertical trajectory. The image of the mosasaur (*Platecarpus*) was created from the outline inferred by *Lindgren et al. (2010)*.

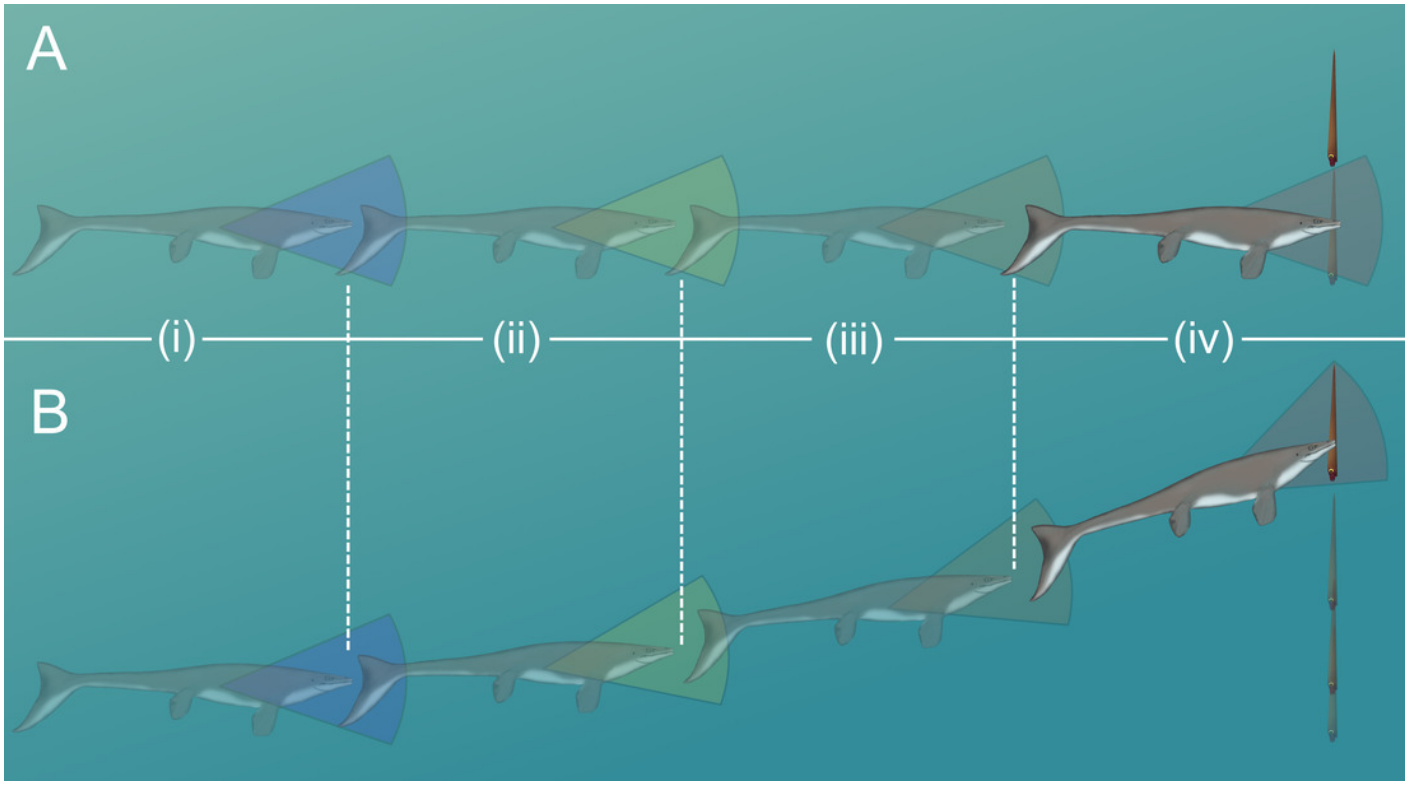

Table 1(on next page)

Model centers of mass and buoyancy.

Local centers of mass for the model components (PLA plastic and bismuth counterweight), and total centers of mass and buoyancy for each model (1: *Nautilus*-like cruising thrust; 2: *Nautilus*-like cruising thrust scaled by the higher mantle cavity ratio of *Sepia*; 3: *Nautilus*-like peak thrust; 4: Slightly negatively buoyant). Only the x and z values are reported because the virtual model is perfectly symmetrical. All coordinates are measured relative to the same arbitrary datum (located in the center of the aperture).

	PLA		Bismuth		Total center of mass		Center of buoyancy	
Baculite model	x (mm)	z (mm)	x (mm)	z (mm)	x (mm)	z (mm)	x (mm)	z (mm)
1	-2.410	130.020	-0.032	-52.279	-1.810	84.070	-1.958	114.191
2	-2.375	119.742	0.439	-57.934	-1.810	84.070	-1.958	114.191
3	-2.052	100.828	0.245	-58.616	-1.810	84.070	-1.958	114.191
4	-1.767	101.472	-2.366	-57.998	-1.810	84.070	-1.958	114.191

1

Table 2(on next page)

Masses (m) and volumes (V) for the virtual and physical model components.

1: *Nautilus*-like cruising thrust; 2: *Nautilus*-like cruising thrust scaled by the higher mantle cavity ratio of *Sepia*; 3: *Nautilus*-like peak thrust; 4: Slightly negatively buoyant. PLA = 3D printed plastic; Bi = bismuth counterweight; wd = water displaced; Mass def. = mass deficiency required to impart the computed buoyant forces (Table 3); glue = the cyanoacrylate glue used to secure each counterweight. The residual mass in the negatively buoyant experiment (denoted with *) was not weighed, but rather its volume was inserted into the model with a syringe (~0.5 cm^3).

	Virtual							Physical					
Baculite model	V_{PLA} (cm^3)	m_{PLA} (g)	V_{Bi} (cm^3)	m_{Bi} (g)	m_{wd} (g)	m_{total} (g)	Mass def. (g)	m_{PLA} (g)	m_{Bi} (g)	m_{glue} (g)	m_{wd} (g)	m_{total} (g)	Mass def. (g)
1	124.319	155.275	5.651	52.490	212.209	207.765	4.444	157.875	49.737	0.101	212.209	207.713	4.496
2	130.978	163.592	4.437	41.211	212.209	204.803	7.406	162.205	42.518	0.207	212.209	204.930	7.280
3	126.935	158.542	2.018	18.745	212.209	177.287	34.922	158.529	18.612	0.355	212.209	177.496	34.713
4	152.102	189.975	2.453	22.789	212.209	212.764	-0.555	187.063	24.875	0.206	212.209	212.144	-0.5*

1

Table 3 (on next page)

Virtual and actual hydrostatic stabilities (S_t) and thrusts (F), and computed percent errors.

1: *Nautilus*-like cruising thrust; 2: *Nautilus*-like cruising thrust scaled by the higher mantle cavity ratio of *Sepia*; 3: *Nautilus*-like peak thrust; 4: Slightly negatively buoyant.

Baculite model	Virtual S_t	Actual S_t	St error (%)	Target F (N)	Actual F (N)	Thrust error (%)
1	0.505	0.492	-2.57	0.0436	0.0441	1.17
2	0.505	0.499	-1.19	0.0727	0.0714	-1.77
3	0.505	0.483	-4.36	0.3426	0.3405	-0.60
4	0.505	0.454	-10.10	-0.0054	-0.0049	-9.42

1

Table 4(on next page)

Velocities, travel times, and asymptote equation coefficients.

Uncertainty reflects bounds of 95% confidence intervals. The asymptotic velocity (in cm/s) is predicted by coefficient “a” of Equation 6. Coefficient “b” governs the slope. The maximum body lengths per second (Max. bl/s) were computed by dividing velocity by the body length of the models (57 cm). The time required to move one body length (t_{bl}) and half of one body length ($t_{bl/2}$) was computed for each model (1: *Nautilus*-like cruising thrust; 2: *Nautilus*-like cruising thrust scaled by the higher mantle cavity ratio of *Sepia*; 3: *Nautilus*-like peak thrust, coated and uncoated with hydrophobic silicone spray).

Model	a (V asymptote cm/s)	b	Max. bl/s	t_{bl} (s)	$t_{bl/2}$ (s)
1	49.89 ± 0.72	0.4827 ± 0.0116	0.875 ± 0.013	2.633 ± 0.048	1.755 ± 0.032
2	59.79 ± 0.58	0.6476 ± 0.0111	1.049 ± 0.010	2.101 ± 0.026	1.395 ± 0.018
3 (uncoated)	162.2 ± 3.10	1.490 ± 0.045	2.846 ± 0.054	0.826 ± 0.019	0.552 ± 0.013
3 (coated)	139.2 ± 1.50	1.970 ± 0.040	2.442 ± 0.026	0.815 ± 0.012	0.535 ± 0.008

1

Table 5(on next page)

Predator evasion potential of orthocone cephalopods using mostly extant predators as analogues.

Dodges are considered successful (highlighted green) when the minimum distance required to start jetting (D) is less than the body length of a predator (L_p) moving at some incident velocity (V_p). The subscripts in D values refer to different thrust scenarios in the models (1: *Nautilus*-like cruising thrust; 2: *Nautilus*-like cruising thrust scaled by the higher mantle cavity ratio of *Sepia*; 3uc: *Nautilus*-like peak thrust with no coating; 3c: *Nautilus*-like peak thrust, coated in hydrophobic silicone spray). The velocity of *Platecarpus* (denoted by *) is only an estimate of metabolically optimal velocity (*Motani, 2002*), therefore critical/lunge velocity should be much higher.

					Moving one body length (57 cm)				Moving 1/2 body length (28.5 cm)			
Species	**Common name**	**L_p (m)**	**V_p (m/s)**	**Reference**	**D_1 (m)**	**D_2 (m)**	**D_{3uc} (m)**	**D_{3c} (m)**	**D_1 (m)**	**D_2 (m)**	**D_{3uc} (m)**	**D_{3c} (m)**
Platecarpus	Mosasaur	4	0.38*	Motani, 2002	1.00	0.80	0.31	0.31	0.67	0.53	0.21	0.20
Megaptera novaeangliae	Humpback whale	12.7	5	Segre et al., 2020	13.17	10.51	4.13	4.08	8.78	6.98	2.76	2.68
Crocodylus porosus	Saltwater crocodile	5	8	Benga et al., 2010	21.06	16.81	6.61	6.52	14.04	11.16	4.42	4.28
Delphinus delphis	Short-beaked common dolphin	1.8	8	Tanaka et al., 2019	21.06	16.81	6.61	6.52	14.04	11.16	4.42	4.28
Stenella attenuata	Pantropical spotted dolphin	1.86	11	Tanaka et al., 2019	28.96	23.11	9.09	8.97	19.31	15.35	6.07	5.89
Isurus oxyrincus	Shortfin mako shark	2.1	19	Fernandez-Waid et al., 2019	50.03	39.92	15.69	15.49	33.35	26.51	10.49	10.17

1